

## Manipulating the temperature dependence of the thermal conductivity of graphene phononic crystal

This content has been downloaded from IOPscience. Please scroll down to see the full text.

2016 Nanotechnology 27 265702

(<http://iopscience.iop.org/0957-4484/27/26/265702>)

View [the table of contents for this issue](#), or go to the [journal homepage](#) for more

Download details:

IP Address: 111.187.39.81

This content was downloaded on 20/05/2016 at 02:58

Please note that [terms and conditions apply](#).

# Manipulating the temperature dependence of the thermal conductivity of graphene phononic crystal

Shiqian Hu<sup>1</sup>, Meng An<sup>2</sup>, Nuo Yang<sup>2,3</sup> and Baowen Li<sup>4</sup>

<sup>1</sup>Center for Phononics and Thermal Energy Science, School of Physics Science and Engineering, Tongji University, Shanghai 200092, People's Republic of China

<sup>2</sup>Nano Interface Center for Energy (NICE), School of Energy and Power Engineering, Huazhong University of Science and Technology (HUST), Wuhan 430074, People's Republic of China

<sup>3</sup>State Key Laboratory of Coal Combustion, Huazhong University of Science and Technology (HUST), Wuhan 430074, People's Republic of China

<sup>4</sup>Department of Mechanical Engineering, University of Colorado, Boulder, CO 80309, USA

E-mail: [nuo@hust.edu.cn](mailto:nuo@hust.edu.cn) and [Baowen.Li@Colorado.Edu](mailto:Baowen.Li@Colorado.Edu)

Received 10 December 2015, revised 31 March 2016

Accepted for publication 29 April 2016


Published 19 May 2016



CrossMark

## Abstract

By using non-equilibrium molecular dynamics simulations, modulating the temperature dependence of thermal conductivity of graphene phononic crystals (GPnCs) is investigated. It is found that the temperature dependence of thermal conductivity of GPnCs follows  $\sim T^{-\alpha}$  behavior. The power exponents ( $\alpha$ ) can be efficiently tuned by changing the characteristic size of GPnCs. The phonon participation ratio spectra and dispersion relation reveal that the long-range phonon modes are more affected in GPnCs with larger holes ( $L_0$ ). Our results suggest that constructing GPnCs is an effective method to manipulate the temperature dependence of thermal conductivity of graphene, which would be beneficial for developing GPnC-based thermal management and signal processing devices.

 Online supplementary data available from [stacks.iop.org/NANO/27/265702/mmedia](http://stacks.iop.org/NANO/27/265702/mmedia)

Keywords: thermal conductivity, molecular dynamics, temperature dependence, graphene phononic crystal

(Some figures may appear in colour only in the online journal)

## Introduction

Graphene is a two-dimensional hexagonal structure consisting of a single atomic layer of carbon [1]. Because of its excellent thermal, electrical, mechanical, and optical properties, graphene has attracted immense interest and been widely studied. Specifically, it has a superior thermal conductivity [2–6] which raises the exciting prospect of using graphene as a promising candidate for phononic (thermal) devices [7–12].

Due to the heat transfer in graphene, mainly contributed by phonons [5], the thermal conductivity of graphene can be manipulated by the management of phonons. Traditionally, the thermal conductivity of graphene is manipulated through

impurities [13], superlattice structure [14], or defects in the lattice crystal [15–17].

Recently, there has been progress in managing phonons by nanostructured phononic crystals (PnCs) [18–23] which control heat by making use of phononic properties. It heralds the next technological revolution in phononics, such as thermal rectifiers [15, 24–31], optomechanical crystals [32, 33], thermal cloaking [34–38], thermoelectrics [39–43], and thermocrystals [18, 21, 22]. When the characteristic size of nanostructured PnCs is close to the wavelength of phonons, PnCs may manipulate the phonon band structures which leads to the phonon confinement [44–47]. Moreover, coherent interference is another underlying mechanism in manipulating phonons by PnCs [22, 48, 49]. These new

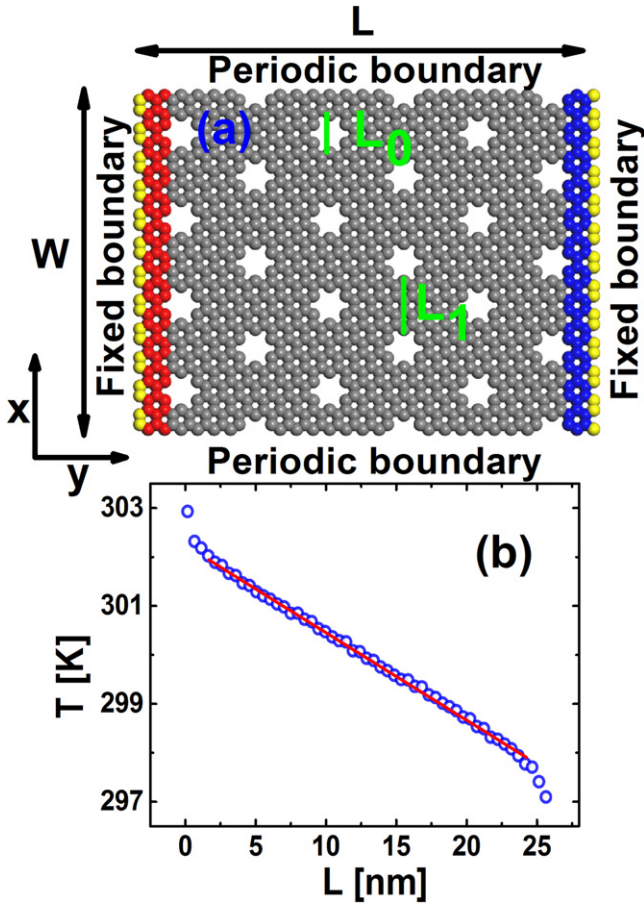


**Figure 1.** (a) Schematic picture of graphene phononic crystal (GPnC). The length (width) of the GPnC is set as  $L$  ( $W$ ).  $L_0$  (size of holes) and  $L_1$  (neck distance) are used to characterize the GPnC structure. (b) The temperature profile of the GPnC. The parameters are  $L = 25$  nm,  $W = 7$  nm,  $L_0 = 0.71$  nm,  $T_0 = 300$  K and  $\Delta = 0.01$ . The temperature gradient is obtained by fitting data excluding the temperature jump at the two ends.

findings are different from traditional methods in managing phonons and have attracted a growing attention.

Efforts have been made to investigate the reduction of thermal conductivity of bulk materials by using a PnC structure. However, the temperature dependence of the thermal conductivity of PnCs has not been investigated systematically and remains confusing, but it is important not only for the theoretical understanding but for applications. In this paper, using non-equilibrium molecular dynamics (NEMD) simulations, modulation of the temperature dependence of the thermal conductivity of GPnCs is investigated. The effect of the size of holes ( $L_0$ ), length ( $L$ ) and neck distance ( $L_1$ ) on thermal conductivity is studied.

### Molecular dynamics simulation methods

As shown in figure 1(a), the GPnC is composed by periodically removing hexagonal holes with a zigzag edge. The size of holes (neck distance) is characterized by  $L_0$  ( $L_1$ ). In calculations, the lattice constant,  $a$ , and thickness of graphene

are chosen as 0.1418 nm and 0.334 nm, respectively. The fixed (periodic) boundary condition is adopted along the longitudinal (transversal) direction. The system along the transversal direction with free boundary conditions corresponds to a nanoribbon where the boundary scattering may have an important effect on the thermal transport, which is not studied here.

In NEMD simulations, in order to establish a temperature gradient, the atoms at two ends are coupled with a Langevin heat bath [50], and whose temperatures are  $T_L$  and  $T_R$  respectively. For convenience, we set the temperatures as  $T_L = T_0 (1 + \Delta)$  and  $T_R = T_0 (1 - \Delta)$ , where  $T_0$  is the average temperature and  $\Delta$  is the normalized temperature difference between the two ends. In studying the dependence of thermal conductivity on temperature,  $T_0$  ranges from 300 K to 1000 K, and  $\Delta$  is fixed as 0.01.

The bonding interaction between carbon atoms is described by the energy potential as a Morse bond and a harmonic cosine angle, which include both two-body and three-body potential terms [26, 51, 52]. We use the velocity Verlet algorithm to integrate the differential equations of motion, where the time step,  $\Delta t$ , is set as 0.5 fs. NEMD simulations are performed at 30 ns in the calculations of the dependence of thermal conductivity on temperature after the system reaches a steady state (description of reaching steady state is shown in supplementary information figure S2, [stacks.iop.org/NANO/27/265702/mmedia](http://stacks.iop.org/NANO/27/265702/mmedia)).

The thermal conductivity ( $\kappa$ ) is calculated based on Fourier's Law as,

$$\kappa = -\frac{J \cdot L}{A \cdot \Delta T} = -\frac{J}{A \cdot \nabla T} \quad (1)$$

where  $J$  is the heat current,  $A$  is the cross section,  $L$  is the length of the simulation cell, and  $\Delta T$  is the temperature difference. The results presented here are averaged from 12 independent simulations from different initial conditions. The error bar is the standard deviations of the results of 12 simulations.

### Molecular dynamics results and discussions

When the width of simulation cell is not sufficiently large, a size effect will occur on the prediction of thermal conductivity [47, 53]. Here, we examined the dependence of thermal conductivity on the width of the simulation cell. The value of  $W$  is increased from 2 nm to 12 nm, while the size of holes  $L_0$  and length  $L$  are fixed as 0.71 nm and 14 nm, respectively. The results show that the thermal conductivity of GPnCs converges when the width is larger than 7 nm (details in supplementary information figure S1). In the following simulations, the width of GPnCs is chosen as 7 nm.

Firstly, the temperature dependence of thermal conductivity is investigated in several GPnC structures whose  $L(W)$  is fixed as 25 nm (7 nm), and  $L_0$  is increased from 0.71 nm to 2.41 nm. Figure 1(b) shows a typical temperature profile of GPnCs. The jumps at the two ends come from the thermal interfacial resistance between the heat baths and the

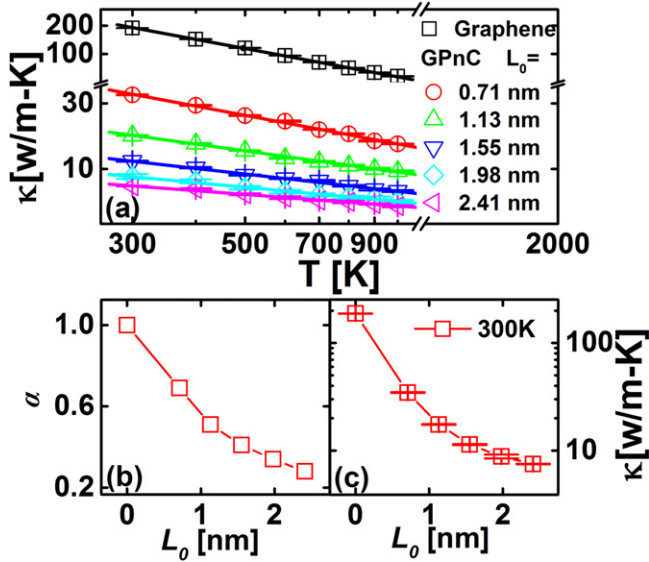


**Figure 2.** (a) Thermal conductivity of graphene and GPnCs with different  $L_0$  versus temperature. The temperature increases from 300 K to 1000 K. The parameters are  $L = 25$  nm,  $W = 7$  nm and  $\Delta = 0.01$ . For GPnCs,  $L_1 = 0.71$  nm and  $L_0$  increases from 0.71 nm to 2.41 nm. The figure is plotted on a log–log scale. The symbols are numerical data and the lines are fitted lines. The fitted values  $\alpha$  are 0.69, 0.51, 0.41, 0.34, 0.28 to corresponding  $L_0$  of 0.71, 1.13, 1.55, 1.98, 2.41 nm, respectively. In particular, for graphene,  $\alpha$  equals 1. (b) The power exponents ( $\alpha$ ) versus  $L_0$ . The values of  $\alpha$  decrease with increasing  $L_0$ . (c) Thermal conductivity of GPnCs versus  $L_0$  at 300 K. The error bar is standard deviation of 12 MD simulations with different initial conditions.

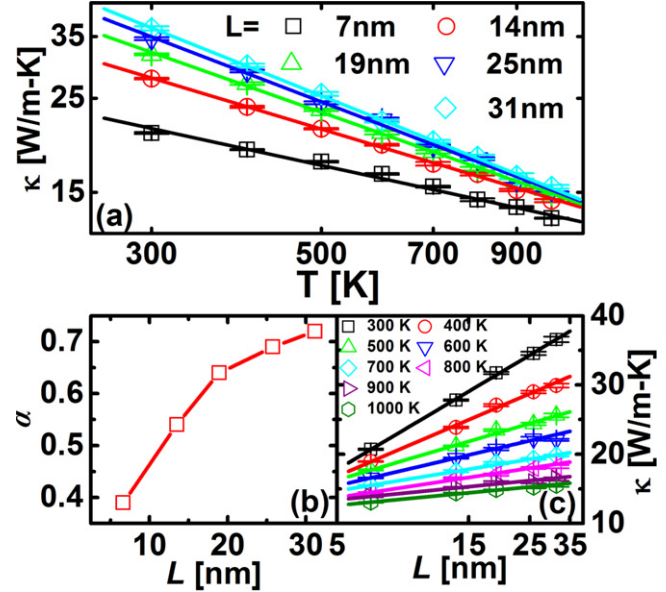


**Figure 3.** (a) Thermal conductivity of GPnCs with different lengths  $L$  versus the temperature. The temperature increases from 300 K to 1000 K. The parameters are  $W = 7$  nm,  $L_1 = 0.71$  nm,  $L_0 = 0.71$  nm and  $\Delta = 0.01$ . The length  $L$  increases from 7 nm to 31 nm. The figure is plotted in a log–log scale. The symbols are numerical data and the lines are fitted lines. The fitted values  $\alpha$  are 0.39, 0.54, 0.63, 0.69 and 0.72 corresponding  $L$  are 7, 14, 19, 25 and 31 nm, respectively. (b) The power exponents ( $\alpha$ ) versus  $L$ . The values of  $\alpha$  decrease as  $L$  decreases. (c) Thermal conductivity of GPnCs versus  $L$  at different temperatures. The symbols are numerical data and the dashed lines are fitted lines. The error bar is standard deviation of 12 MD simulations with different initial conditions.

system. Excluding the effects at these two ends, the data are fitted linearly to obtain the temperature gradient.

The results of temperature dependence of thermal conductivity are shown in figure 2(a). For convenience of comparison, figure 2(a) shows the thermal conductivity of both graphene ( $\kappa_G$ ) and GPnCs ( $\kappa_{\text{GPnCs}}$ ) with the same length,  $L$ , as 25 nm. It is found that both  $\kappa_G$  and  $\kappa_{\text{GPnCs}}$  decrease with the temperature increasing as  $\sim T^{-\alpha}$  due to the Umklapp phonon–phonon scattering. Graphene has a  $T^{-1}$  behavior followed a Slack relation [54], which is consistent with previous work [47]. However, GPnCs have different power exponent,  $\alpha$ , corresponding to its size of holes,  $L_0$ . The results show that the values of  $\alpha$  are 0.69, 0.51, 0.41, 0.34 and 0.28 corresponding to  $L_0$  as 0.71, 1.13, 1.55, 1.98 and 2.41 nm, respectively. Namely, the value of  $\alpha$  decreases with the increase of  $L_0$  (shown in figure 2(b)). It is known that the Slack relation is valid only when the long-range acoustic phonons dominate the thermal transport, while both short-range acoustic and optical phonons are not important [54, 55]. This precondition is sometimes not satisfied for structures with low thermal conductivity, such as zeolites [56] and GPnCs in our work.

As shown in figure 2(a), compared with the thermal conductivity of graphene,  $\kappa_{\text{GPnCs}}$  significantly decreases and has less of a dependence on temperature. It has been demonstrated that the thermal conductivity contributed by short-range acoustic and optical phonons is temperature-

independent in previous works [56, 57]. In graphene, the long-range acoustic phonons dominate the thermal transport [58]. The significant decrease of thermal conductivity of GPnCs and a less sensitive dependence on temperature is probably caused by the affected long-range acoustic phonons.

Moreover, as shown in figure 2(a),  $\kappa_{\text{GPnCs}}$  decreases with increasing  $L_0$  over a large temperature range (300 K to 1000 K). For instance, when  $L_0$  equals 2.41 nm,  $\kappa_{\text{GPnCs}}$  is reduced to 4% of  $\kappa_G$  at room temperature. The  $\kappa_{\text{GPnCs}}$  with different  $L_0$  at room temperature are shown in figure 2(c). The lower group velocities, due to the flatted phonon dispersion curves (details in figures 5(b) and (c)) and phonon modes more localized in GPnCs with larger  $L_0$  (details in figure 5(a)), are likely responsible for its lower thermal conductivity.

Besides the size of holes ( $L_0$ ), the length of GPnCs ( $L$ ) is another characteristic length affecting the temperature dependence of  $\kappa_{\text{GPnCs}}$ . We fix  $L_0$  as 0.71 nm and meanwhile change  $L$  from 7 nm to 31 nm. The thermal conductivity results are shown in figure 3(a). It is found that  $\kappa_{\text{GPnCs}}$  also follows  $\sim T^{-\alpha}$  behavior. The values of  $\alpha$  are 0.39, 0.54, 0.63, 0.69 and 0.72 corresponding  $L$  are 7, 14, 19, 25 and 31 nm, respectively. Essentially, the power exponents ( $\alpha$ ) decreases with decreasing  $L$  (shown in figure 3(b)). When the system size ( $L$ ) decreases, the confinement of size effects on long-range phonons become stronger compared with the short-

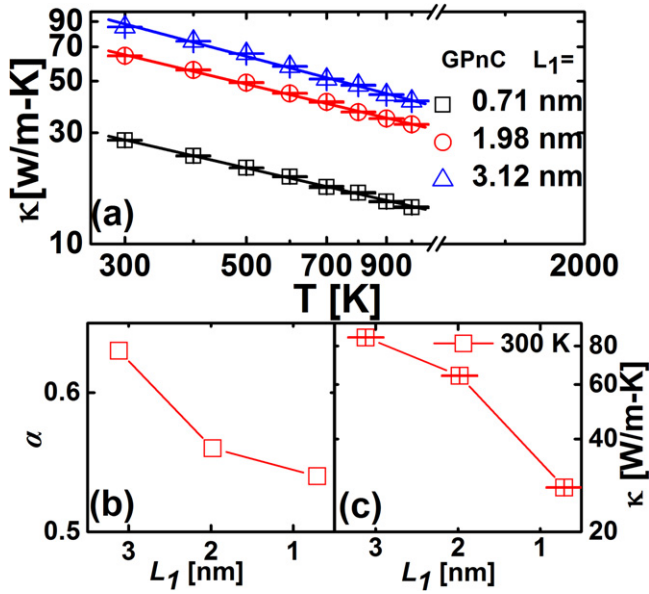


**Figure 4.** (a) Thermal conductivity of GPnCs with different  $L_1$  versus the temperature. The temperature increases from 300 K to 1000 K. The parameters are  $L = 14$  nm,  $W = 7$  nm and  $\Delta = 0.01$ . For GPnCs,  $L_0 = 0.71$  nm and  $L_1$  increases from 0.71 nm to 3.12 nm. The figure is plotted on a log–log scale. The symbols are numerical data and the lines are fitted lines. The fitted values  $\alpha$  are 0.62, 0.57, 0.54 corresponding to  $L_1$  of 3.12, 1.98, 0.71 nm, respectively. (b) The power exponents ( $\alpha$ ) of GPnCs versus  $L_1$ . The values of  $\alpha$  decrease with decreasing  $L_1$ . (c) Thermal conductivity of GPnCs versus  $L_1$  at 300 K. The error bar is the standard deviation of 12 MD simulations with different conditions.

range phonons. As a result, most of the long-range phonons are suppressed. In this case, it is possible to have a ‘reversal effect’, in which the contribution of short-range acoustic phonons and optical phonons to thermal conductivity become larger. That leads to the reduction of the value of  $\alpha$  [56, 57]. This result indicates that the value of  $\alpha$  could be effectively tuned by changing the length of GPnCs.

In addition, as shown in figure 3(c),  $\kappa_{\text{GPnCs}}$  diverges with increasing  $L$  as a  $\log(L)$  behavior in a large temperature range (300 K to 1000 K). It exhibits the same behavior as  $\kappa_G$ , which has been found in experimental study [5]. This result shows a consequence of the two-dimensional nature of phonons in GPnCs, and provides strong evidence that Fourier’s law of heat conduction is not valid in two-dimensional nanostructures, just as in one-dimensional nanostructures [59].

Moreover, the effect of neck distance ( $L_1$ ), another characteristic length of the GPnCs, on the thermal conductivity of GPnCs is investigated. The  $L$  ( $L_0$ ) is fixed as 14 nm (0.71 nm), while  $L_1$  is increased from 0.71 nm to 3.12 nm. The thermal conductivity results are shown in figure 4(a). It is found that the thermal conductivity of GPnCs also has a power relation with  $T$  as  $T^{-\alpha}$ . The values of  $\alpha$  are 0.62, 0.57, and 0.54 corresponding to  $L_1$  of 3.12, 1.98, and 0.71 nm, respectively. The power exponent ( $\alpha$ ) decreases with decreasing  $L_1$  (shown in figure 4(b)). As shown in figure 4(a),  $\kappa_{\text{GPnCs}}$  decreases with decreasing  $L_1$  in a large temperature range (300 K to 1000 K). The  $\kappa_{\text{GPnCs}}$  with different  $L_1$  at room temperature are shown in figure 4(c). In our

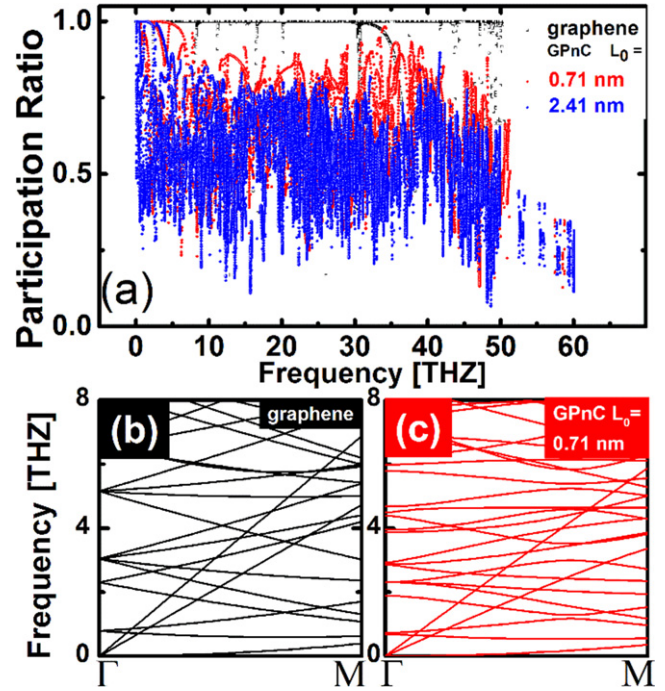


**Figure 5.** (a) Participation ratio spectra of graphene and GPnCs with different  $L_0$  (0.71 nm or 2.41 nm). Black points correspond to participation ratios of graphene. Red points and blue points correspond to participation ratio of GPnCs with  $L_0$  0.71 nm and 2.41 nm, respectively. GPnCs have a smaller participation ratio than graphene. Additionally, GPnCs with smaller  $L_0$  have a larger participation ratio. (b) The low frequency part of the phonon dispersion curves of the GPnC along the  $\Gamma$ -M direction. (c) The low frequency part of the phonon dispersion curves of the GPnC along the  $\Gamma$ -M direction. The square graphene cell in (b) and the GPnC in (c) are the same as the graphene cell in (a), and the size of holes  $L_0$  in the GPnC is 0.71 nm. Phonon dispersions in the GPnC are flattened compared with those in graphene.

previous works [46, 47], it is found that PnCs with large porosity (corresponding to large  $L_1$  in this work) have lower group velocities and more localizations. The lower group velocities and more localizations, due to the  $L_1$  decreasing, are probably responsible for the decreasing of power exponents ( $\alpha$ ). This result indicates that the value of  $\alpha$  could be effectively tuned by changing the neck distance.

In order to understand the underlying physical mechanism of the reduction of power exponent,  $\alpha$ , the participation ratio spectra and dispersion relation of graphene and GPnCs are calculated (shown in figure 5). The participation ratio ( $P$ ) of phonon mode  $k$  is defined by the normalized eigenvector  $\varepsilon_{i\alpha,k}$

$$p_k = \frac{1}{N \sum_{i=1}^N \left( \sum_{\alpha=1}^3 \varepsilon_{i\alpha,k}^* \varepsilon_{i\alpha,k} \right)^2} \quad (2)$$

where  $N$  is the total number of atoms and  $\varepsilon_{i\alpha,k}$  is calculated by the general utility lattice program (GULP) [60]. When there are fewer atoms participating in the motion, the phonon mode has a smaller value of  $P$ .

As shown in figure 5(a), the participation ratios of GPnCs are significantly reduced compared with those of graphene,

thus phonon modes of GPnCs are more localized (a smaller relaxation time) than graphene. Additionally, there exists a further reduction of the participation ratios in GPnCs when  $L_0$  changes from 0.71 nm to 2.41 nm, which means that a larger  $L_0$  could enhance phonon localizations in GPnCs, i.e with increasing  $L_0$ , the phonon relaxation time of GPnCs decreases. Figures 5(b) and (c) show the lower-frequency part of phonon dispersion of graphene and GPnCs. The phonon dispersions of graphene and GPnCs along the transverse direction, from  $\Gamma$  (0, 0, 0) to  $M$  (1, 0, 0) (details of high-symmetry points shown in figure S3 of supplementary information), are calculated by lattice dynamics implemented in GULP [60]. However, considering the fact that in-plane heat transport in graphene is isotropic [61], only zigzag graphene and zigzag GPnCs are studied in this work. Obviously, the phonon dispersions are folded and flattened in GPnCs, thus the group velocity is significantly decreased, especially for the acoustic phonons. In GPnCs, combining the phonon relaxation time and group velocity effect with the  $L_0$  increase, the long-range acoustic phonons will be suppressed, thus the relative contribution from the short-range acoustic and optical phonons to  $\kappa_{\text{GPnCs}}$  increases compared with that in the case of graphene, which violates the valid condition of the Slack relation and leads to a less sensitive dependence on temperature.

## Summary

In summary, we have studied the modulation of temperature dependence of the thermal conductivity of GPnCs by using NEMD simulations. The results show that, compared to graphene, the thermal conductivity of GPnCs has less of a dependence on temperature. There is a relationship of  $\kappa_{\text{GPnCs}} \sim T^{-\alpha}$  where the value of  $\alpha$  can be tuned by changing the characteristic length of GPnCs, such as  $L_0$ ,  $L_1$  and  $L$ . Our results demonstrate that constructing a GPnCs structure is an effective way to tune the temperature dependence of  $\kappa_{\text{GPnCs}}$ . The ability to tune and control the temperature dependence of thermal conductivity of GPnCs provides potential ways to thermally design GPnCs-based signal devices at the nanoscale.

## Acknowledgments

This project was supported in part by grants from the National Natural Science Foundation of China: 11334007 and 51576076. We are grateful to Nianbei Li, Qichen Song, Dengke Ma, Zelin Jin, Weiwei Zhu, Biao Wang, Tingyu Lu for useful discussions. The authors thank the National Supercomputing Center in Tianjin (NSCC-TJ) for providing assistance in computations.

## References

- [1] Novoselov K, Geim A K, Morozov S, Jiang D, Grigorieva M K I, Dubonos S and Firsov A 2005 *Nature* **438** 197
- [2] Balandin A A, Ghosh S, Bao W, Calizo I, Teweldebrhan D, Miao F and Lau C N 2008 *Nano Lett.* **8** 902
- [3] Ghosh S, Calizo I, Teweldebrhan D, Pokatilov E P, Nika D L, Balandin A A, Bao W, Miao F and Lau C N 2008 *Appl. Phys. Lett.* **92** 151911
- [4] Lee J-U, Yoon D, Kim H, Lee S W and Cheong H 2011 *Phys. Rev. B* **83** 081419
- [5] Xu X et al 2014 *Nat. Commun.* **5** 3689
- [6] Kong B D, Paul S, Nardelli M B and Kim K W 2009 *Phys. Rev. B* **80** 033406
- [7] Li B W, Wang L and Casati G 2006 *Appl. Phys. Lett.* **88** 143501
- [8] Wang L and Li B 2007 *Phys. Rev. Lett.* **99** 177208
- [9] Ai B Q, Zhong W R and Hu B B 2012 *J. Phys. Chem. C* **116** 13810
- [10] Ai B Q, An M and Zhong W R 2013 *J. Chem. Phys.* **138** 034708.
- [11] Ben-Abdallah P and Biehs S A 2014 *Phys. Rev. Lett.* **112** 044301
- [12] Han H, Li B, Volz S and Kosevich Y A 2015 *Phys. Rev. Lett.* **114** 145501
- [13] Chen S, Wu Q, Mishra C, Kang J, Zhang H, Cho K, Cai W, Balandin A A and Ruoff R S 2012 *Nat. Mater.* **11** 203
- [14] Ouyang T, Chen Y P, Yang K K and Zhong J X 2009 *EPL* **88** 28002
- [15] Hu J, Ruan X and Chen Y P 2009 *Nano Lett.* **9** 2730
- [16] Haskins J, Kınacı A, Sevik C, Sevinçli H, Cuniberti G and Çağın T 2011 *ACS Nano* **5** 3779
- [17] Fthenakis Z G, Zhu Z and Tománek D 2014 *Phys. Rev. B* **89** 125421
- [18] Yu J K, Mitrovic S, Tham D, Varghese J and Heath J R 2010 *Nat. Nanotechnol.* **5** 718
- [19] Tang J, Wang H T, Lee D H, Fardy M, Huo Z, Russell T P and Yang P 2010 *Nano Lett.* **10** 4279
- [20] Hopkins P E, Reinke C M, Su M F, Olsson R H, Shaner E A, Leseman Z C, Serrano J R, Phinney L M and El-Kady I 2011 *Nano Lett.* **11** 107
- [21] Maldovan M 2013 *Nature* **503** 209
- [22] Maldovan M 2013 *Phys. Rev. Lett.* **110** 025902
- [23] Lee J, Lim J and Yang P 2015 *Nano Lett.* **15** 3273
- [24] Li N B, Ren J, Wang L, Zhang G, Hanggi P and Li B W 2012 *Rev. Mod. Phys.* **84** 1045
- [25] Yang N, Li N, Wang L and Li B 2007 *Phys. Rev. B* **76** 020301
- [26] Yang N, Zhang G and Li B 2008 *Appl. Phys. Lett.* **93** 243111
- [27] Yang N, Zhang G and Li B 2009 *Appl. Phys. Lett.* **95** 033107
- [28] Li B, Wang L and Casati G 2004 *Phys. Rev. Lett.* **93** 184301
- [29] Chang C, Okawa D, Majumdar A and Zettl A 2006 *Science* **314** 1121
- [30] Liu Y-Y, Zhou W-X, Tang L-M and Chen K-Q 2014 *Appl. Phys. Lett.* **105** 203111
- [31] Liu Y Y, Zhou W X and Chen K Q 2015 *Sci. Rep.* **5** 17525
- [32] Eichenfield M, Chan J, Camacho R M, Vahala K J and Painter O 2009 *Nature* **462** 78
- [33] Safavi-Naeini A H, Hill J T, Meenehan S, Chan J, Groblacher S and Painter O 2014 *Phys. Rev. Lett.* **112** 153603
- [34] Han T, Bai X, Thong J T, Li B and Qiu C W 2014 *Adv. Mater.* **26** 1731
- [35] Narayana S, Savo S and Sato Y 2013 *Appl. Phys. Lett.* **102** 201904
- [36] Guenneau S, Amra C and Veynante D 2012 *Opt. Express* **20** 8207
- [37] Han T, Bai X, Gao D, Thong J T, Li B and Qiu C W 2014 *Phys. Rev. Lett.* **112** 054302

- [38] Han T, Yuan T, Li B and Qiu C W 2013 *Sci. Rep.* **3** 1593
- [39] Chen G, Dresselhaus M S, Dresselhaus G, Fleurial J P and Caillat T 2003 *Int. Mater. Rev.* **48** 45
- [40] Dresselhaus M S, Chen G, Tang M Y, Yang R G, Lee H, Wang D Z, Ren Z F, Fleurial J P and Gogna P 2007 *Adv. Mater.* **19** 1043
- [41] Vineis C J, Shakouri A, Majumdar A and Kanatzidis M G 2010 *Adv. Mater.* **22** 3970
- [42] Jin Z, Liao Q, Fang H, Liu Z, Liu W, Ding Z, Luo T and Yang N 2015 *Sci. Rep.* **5** 18342
- [43] Yang L, Yang N and Li B 2016 *Int. J. Heat Mass Transfer* **99** 102–6
- [44] Balandin A and Wang K L 1998 *Phys. Rev. B* **58** 1544
- [45] Yang L, Yang N and Li B 2013 *Sci. Rep.* **3** 1143
- [46] Yang L, Yang N and Li B 2014 *Nano Lett.* **14** 1734
- [47] Yang L N, Chen J, Yang N and Li B W 2015 *Int. J. Heat Mass Transfer* **91** 428
- [48] Zen N, Puurtinen T A, Isotalo T J, Chaudhuri S and Maasilta I J 2014 *Nat. Commun.* **5** 3435
- [49] Alaie S, Goettler D F, Su M, Leseman Z C, Reinke C M and El-Kady I 2015 *Nat. Commun.* **6** 7228
- [50] Yang N, Zhang G and Li B 2008 *Nano Lett.* **8** 276
- [51] Quo Y, Karasawa N and Goddard W A 1991 *Nature* **351** 464
- [52] Tuzun R E, Noid D W, Sumpter B G and Merkle R C 1996 *Nanotechnology* **7** 241
- [53] Schelling P K, Phillpot S R and Keblinski P 2002 *Phys. Rev. B* **65** 144306
- [54] Slack G A 1979 *Solid State Phys.* **34** 1
- [55] Kaviany M 2008 (New York: Cambridge University Press) p 212
- [56] McGaughey A and Kaviany M 2004 *Int. J. Heat Mass Transfer* **47** 1799
- [57] McGaughey A J H and Kaviany M 2004 *Int. J. Heat. Mass Transfer* **47** 1783
- [58] Feng T L, Ruan X L, Ye Z Q and Cao B Y 2015 *Phys. Rev. B* **91** 224301
- [59] Yang N, Zhang G and Li B 2010 *Nano Today* **5** 85
- [60] Gale J D 1997 *J. Chem. Soc. Faraday Trans.* **93** 629
- [61] Chen J, Zhang G and Li B 2013 *Nanoscale* **5** 532